

Electronic Supplementary Information for:

Tailoring Au-core Pd-shell Pt-cluster Nanoparticles for Enhanced Electrocatalytic Activity

⁵ Ping-Ping Fang,^a Sai Duan,^a Xiao-Dong Lin,^a Jason R. Anema,^a Jian-Feng Li,^a Olivier Buriez,^b Yong Ding,^c Feng-Ru Fan,^a De-Yin Wu,^a Bin Ren,^a Zhong Lin Wang,^c Christian Amatore,^b and Zhong-Qun Tian^{a*}

^a State Key Laboratory of Physical Chemistry of Solid Surfaces and LIA CNRS XiamENS "NanoBioChem", College of Chemistry and Chemical

Engineering, Xiamen University, Xiamen 361005, China. Fax: + 86 592 2183047; Tel: + 86 592 2186979; E-mail: zqtian@xmu.edu.cn

^b UMR CNRS 8640 "PASTEUR" and LIA CNRS XiamENS "NanoBioChem", Ecole Normale Supérieure, Département de Chimie, Université Pierre et Marie Curie-Paris 6, 24 rue Lhomond, 75231 Paris cedex 05, France.

^cSchool of Materials Science and Engineering, Georgia Institute of Technology, Atlanta, Georgia 30332, USA.

¹⁵ **S1 Additional TEM and HRTEM images of 16 nm Au@Pd@Pt NPs, and evidence for a distinct core-shell-cluster structure over an alloy structure**

The size of the Au core, the thickness of the Pd shell and the coverage of the Pt clusters are all tuneable. Some TEM and ²⁰ HRTEM images of 16 nm Au@Pd@Pt NPs are provided in Figure S1. These NPs were loaded onto carbon black as described in section S2 of the electronic supporting information (ESI), and their catalytic activities were normalized by the mass of Pt and Pd. The results obtained were similar to those presented in Figure 4 ²⁵ of the main text: NPs coated with 2 atomic layers of Pd and a half-monolayer equivalent of Pt ($\theta_{\text{Pt}} \approx 0.5$) displayed the highest catalytic activity for the electrooxidation of formic acid.

The epitaxial growth mode for Pd on Au is well established.¹⁻² There have also been some reports of an epitaxial rather than ³⁰ alloy Pd-Pt interface for Pd@Pt nanocubes,³⁻⁵ and of island growth for Pt on Au.⁶ In the present study we have found that Pt cannot grow epitaxially on Au@Pd NPs with 2-3 monolayers of Pd because the Pd surface has the lattice structure of Au and because the cohesive energy of Pt is very high. In regard to the ³⁵ possible formation of an alloy between our Au core and our Pd shell, recent papers from our group show that when Au NPs are coated with a single atomic layer of Pd, the strain between them is released by Shockley partial dislocations (SPDs) accompanied by the formation of stacking faults. For NPs coated with > 2 nm ⁴⁰ of Pd, the stacking faults still exist but no SPDs are found. The elimination of SPDs may result from diffusion of Au atoms into the Pd shell.⁷ Thus, an alloy may well form between Au and Pd when the Pd shell is > 2 nm, but not when it is only 2 atomic layers thick. Based on the above reports, the seed-mediated ⁴⁵ growth method that we used and our experimental results, it is quite reasonable to say that our Au@Pd@Pt NPs possess a distinct Au-core Pd-shell Pt-cluster structure instead of an alloy one. Finally, the Pt island structure can be seen in ESI Figure S1B and main text Figure 2I.

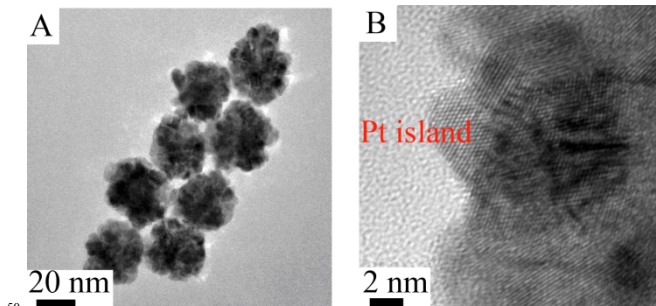


Figure S1. TEM (A) and HRTEM (B) images of 16 nm Au@Pd@Pt NPs with 2 atomic layers of Pd and $\theta_{\text{Pt}} \approx 20$.

⁵⁰ **S2 The procedure for loading 9 nm Ag@Pd@Pt NPs onto carbon black, and an SEM image**

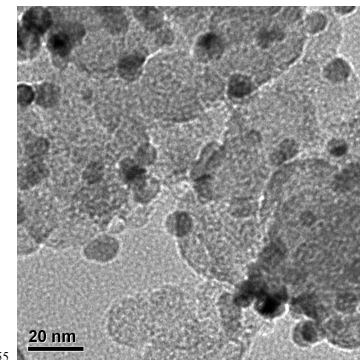


Figure S2. SEM image of 9 nm Ag@Pd@Pt NPs on carbon black.

Ag NPs with an average diameter of 9 nm were synthesized according to the literature.⁸ Ag@Pd@Pt NPs were then prepared ⁶⁰ by a method similar to the one used to make Au@Pd@Pt NPs. Carbon black (Vulcan XC-72, Cabot Corporation) was dispersed in water by sonicing for at least 30 min, then some of the resulting suspension was added into the Ag@Pd@Pt NP solution to give a metal loading of 10 wt% (counting only the mass of Pd ⁶⁵ and Pt) and this mixture was sonicated for another 30 min. A centrifuge-based washing procedure was performed 3 times. Next, the carbon-supported Ag@Pd@Pt NPs were thermally treated at 150 °C for 8 h in air. 3 mg of each sample were placed in a 270 µL / 30 µL Nafion (0.25%) solution and sonicated until ⁷⁰ the formation of a well-dispersed ink. 3 µL of this ink were

dropped onto a glassy carbon (GC) electrode and dried under vacuum. Coverage of the catalyst on the GC electrode was 424 $\mu\text{g}/\text{cm}^2$. An SEM image is provided in Figure S2.

S3 Verifying the band assignments for adsorbed CO by examining Au@Pd and Au@Pt NPs

The SERS spectra of CO adsorbed on Au@Pd and Au@Pt surfaces are shown in Figure S3. We “borrowed” SERS activity from the Au core to observe CO on the Pd or Pt metal.⁹⁻¹⁰

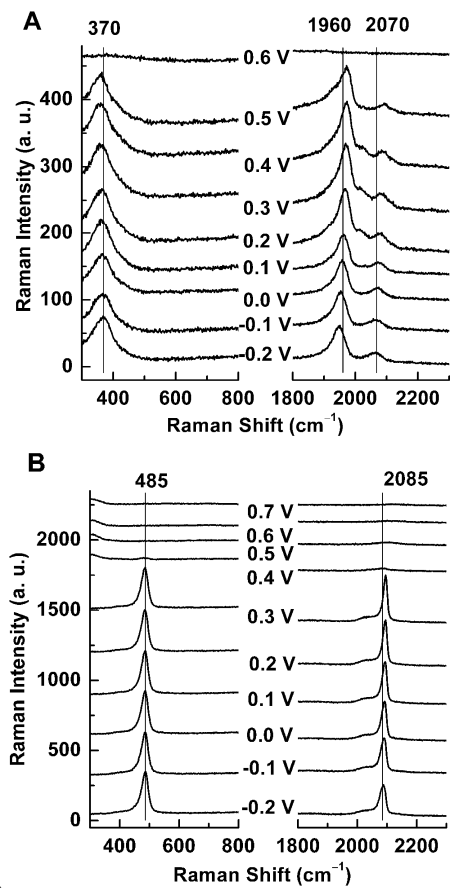


Figure S3. SERS spectra of CO adsorbed on two different substrates in a CO-saturated 0.1 M aqueous solution of H_2SO_4 at different potentials: (A) 55 nm Au@Pd NPs with 2 monolayers of Pd, and (B) 55 nm Au@Pt NPs with $\theta_{\text{Pt}} \approx 2$.

When CO is adsorbed on 55 nm Au@Pd NPs with 2 monolayers of Pd (Figure S3A), the most notable features are the strong band at about 1960 cm^{-1} and the weak band at about 2070 cm^{-1} , which are attributed to the C-O stretching mode of bridge- and linear-bonded CO atoms respectively.¹¹ A single broad band at about 370 cm^{-1} appears in the low-frequency region, and it is assigned to the Pd-C vibration of bridge-bonded CO.¹²

When CO is adsorbed on 55 nm Au@Pt NPs with $\theta_{\text{Pt}} \approx 2$ (Figure S3B), bands appear at about 2085 cm^{-1} in the high-frequency region and about 485 cm^{-1} in the low-frequency region. These bands are attributed to linear-bonded CO on Pt, and the Pt-C vibration respectively.¹¹⁻¹² Some of the CO is bridge-bonded; however, it has been shown that CO adsorption occurs mainly on Pt top sites and this is the case even for rough Pt surfaces, which

has been illustrated in the literature by *in situ* surface enhanced Raman spectroscopy and Time-Resolved Infrared Study.¹³⁻¹⁴

The Pd band positions at 1960 and 370 cm^{-1} here match those at 1950 and 375 cm^{-1} in Figure 6B; and the Pt ones at 2085 and 485 here match those at 2074 and 482 in Figure 6B. The frequency shifts associated with changes in applied potential (Figure S3) are due to an electrochemical Stark effect, which has been illustrated in the literature by *in-situ* Fourier transform infrared spectroscopy and *in-situ* Fourier transform infrared spectroscopy.¹⁵⁻¹⁶

S4 Cyclic voltammograms obtained from Au@Pd@Pt NPs

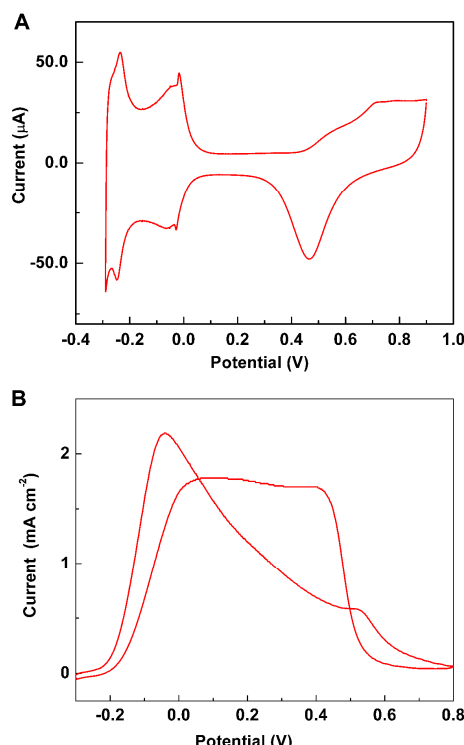


Figure S4. (A) Cyclic voltammograms obtained from 55 nm Au@Pd@Pt NPs with 2 monolayers of Pd and $\theta_{\text{Pt}} \approx 0.5$ in 0.1 M H_2SO_4 (A) and 0.1 M $\text{HCOOH} + 0.1 \text{ M H}_2\text{SO}_4$ (B). The scanning rate was 50 mV/s.

Cyclic voltammograms (CVs) obtained for 55 nm Au@Pd@Pt NPs with 2 monolayers of Pd and $\theta_{\text{Pt}} \approx 0.5$, in the absence of formic acid, are presented in Figure S4A. The desorption peaks for weakly adsorbed hydrogen may be seen at about -0.23 V, and the ones for strongly adsorbed hydrogen may be seen at about -0.02 V. Now Figure 4A (black curve) in the main text shows that formic acid oxidation begins to take place at about -0.23 V and reaches a maximum at about -0.05 V. Taking into consideration the fact that the scanning rates are different, these two pairs of potentials match quite well and suggest formic acid oxidation is closely tied to hydrogen desorption: when this poison is removed, active sites are left free for the electrooxidation of the formic acid.

Voltammetric profiles recorded for oxidation of formic acid on the same Au@Pd@Pt NPs are displayed in Figure S4B. In the potential region below 0.1 V, currents in the positive scan

are higher than those in the negative scan, thus suggesting a lack of surface poisoning in the initial positive scan. The differences in current density for the negative scan with respect to the positive one have been tentatively associated with the reduction of CO_2 , which forms at positive potentials, to CO on Pt.¹⁷⁻¹⁹ Feliu¹⁸ and co-workers have studied the reduction of CO_2 to CO in detail by differential electrochemical mass spectrometry (DEMS).

S5 Chronoamperometric analyses of the catalytic activity and stability of our Au@Pd@Pt NPs

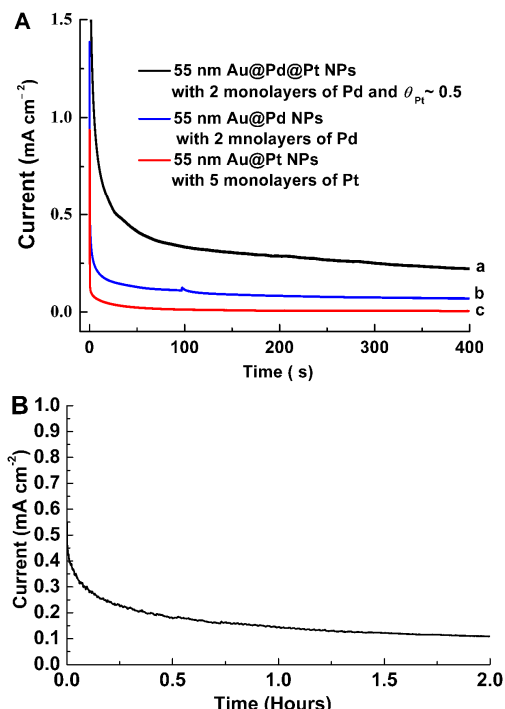


Figure S5. (A) Chronoamperometric curves for 55 nm Au@Pd@Pt NPs with 2 monolayers of Pd and $\theta_{\text{Pt}} \approx 0.5$ (a), 55 nm Au@Pd NPs with 2 monolayers of Pd (b), and 55 nm Au@Pt NPs with 5 monolayers of Pt (c). (B) A chronoamperometric curve for 55 nm Au@Pd@Pt NPs with 2 monolayers of Pd and $\theta_{\text{Pt}} \approx 0.5$. The potential was stepped from $E_{\text{initial}} = -0.30$ V to $E_{\text{final}} = 0.00$ V and held there for 400 s (A) or 2 hours (B). All of these experiments were carried out in a 0.1 M HCOOH + 0.1 M H_2SO_4 solution.

To further evaluate the activity and stability of our NP catalysts, chronoamperometric analyses were carried out by stepping the potential from $E_{\text{initial}} = -0.30$ V to $E_{\text{final}} = 0.00$ V, and then holding at 0.00 V for 400 s (Figure S5A) or 2 hours (Figure S5B), in 0.1 M HCOOH + 0.1 M H_2SO_4 . The E_{final} value of 0.00 V corresponds to the potential of maximum formic acid oxidation activity (Figure 4, black curves). It can be seen in Figure S5A that the maximum initial and steady state oxidation current densities were obtained from the 55 nm Au@Pd@Pt NPs with 2 monolayers of Pd and $\theta_{\text{Pt}} \approx 0.5$, followed by the 55 nm Au@Pd NPs with 2 monolayers of Pd and 55 nm Au@Pt NPs with 5 monolayers of Pt. All these systems were found to be stable with respect to time.

S6 SERS spectra showing electrooxidation of formic acid on 55 nm Au@Pd NPs with 2 monolayers of Pd

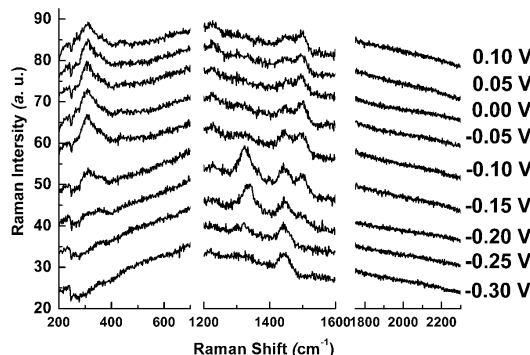


Figure S6. SERS spectra obtained from 55 nm Au@Pd NPs with 2 monolayers of Pd on a GC electrode in 0.1 M H_2SO_4 containing 1 M HCOOH. Each potential is indicated in the figure.

Figure S6 shows that at potentials negative of -0.25 V, there is one peak at 1444 cm⁻¹ which may be attributed to citrate adsorbed on the NPs. From -0.20 V to -0.15 V, a peak is observed at 1325 cm⁻¹, and it has been assigned to bridge-bonded formate by Chen et al.²⁰ and Samjeske²¹ et al. At potentials ≥ -0.20 V, a peak at 1498 cm⁻¹ appears together with a peak at about 309 cm⁻¹ in the low wavenumber region, and these may be assigned to H-O-C which is generated during the oxidation of formic acid.²² The most notable result is that there is no CO produced during formic acid oxidation on a pure Pd surface, as there is no C-O band in the high frequency region.

S7 DFT calculations for the adsorption energy of COOH

Since the DFT results in Table 1 indicate D-sites are not poisoned by CO, and thus free to catalyze the electrooxidation of formic acid, we decided to calculate the adsorption energy for a reaction intermediate at the D-site to illustrate its competition with CO there. We considered both COOH and HCOO initially, but DFT calculations for testing adsorbate stability showed COOH to be more stable than HCOO by about 0.4 eV. Since the former of these was found to be so much more stable than the latter, adsorption energies were not calculated for HCOO and we focused our attention exclusively on COOH. No attempt was made to simulate the electrochemical potentials, since it has been shown that local coverage of the surface species affected by the potential is more important than variations in the electric field at an electrode when modeling formic acid adsorption and reactions.

The hydrogen has two possible orientations: away from the surface (up, COOH_u) and toward the surface (down, COOH_d). For the Au@Pd@Pt NPs with 2 monolayers of Pd, the adsorption energy of COOH_u is 2.13 eV and the adsorption energy of COOH_d is 2.30 eV. For the Au@Pd@Pt NPs with 5 monolayers of Pd, we calculated 2.11 eV for COOH_u and 2.26 eV for COOH_d. In both the 2 monolayer and the 5 monolayer cases, the adsorption energy of COOH_d is greater than the adsorption

energy of COOH_u, indicating that COOH tends to favor down-side adsorption. According to Cai²³ and coworkers, down-side adsorption greatly facilitates the direct oxidization of formic acid to CO₂, meaning higher catalytic activity. Our calculations also show that moving from 2 to 5 monolayers of Pd has little effect on COOH adsorption: the two numbers for COOH_u are similar and the two numbers for COOH_d are similar. These values for COOH may be compared with the values for CO given in Table 1: 1.57 eV for adsorption on Au@Pd@Pt NPs with 2 monolayers of Pd, and 1.84 eV for adsorption on similar NPs having 5 monolayers of Pd. The two adsorption energies for CO are not similar, and they show that CO poisoning is a greater problem for Au@Pd@Pt NPs with 5 monolayers of Pd than for Au@Pd@Pt NPs with 2 monolayers of Pd. Again, this difference in catalytic activity may be caused by geometrical effects or differing positions of the Au core d-band center for 2 and 5 monolayers of Pd.

References.

- 1 P. H. C. Camargo, Y. Xiong, L. Ji, J. M. Zuo, Y. Xia, *J. Am. Chem. Soc.* 2007, **129**, 15452.
- 2 Y. J. Xiang, X. C. Wu, D. F. Liu, X. Y. Jiang, W. G. Chu, Z. Y. Li, Y. Ma, W. Y. Zhou, S. S. Xie, *Nano Lett.* 2006, **6**, 2290.
- 3 S. E. Habas, H. Lee, V. Radmilovic, G. A. Somorjai, P. Yang, *Nat. Mater.* 2007, **6**, 692.
- 4 H. J. Lee, S. E. Habas, G. A. Somorjai, P. D. Yang, *J. Am. Chem. Soc.* 2008, **130**, 5406.
- 5 B. Lim, J. G. Wang, P. H. C. Camargo, M. J. Jiang, M. J. Kim, Y. N. Xia, *Nano Lett.* 2008, **8**, 2535.
- 6 F. R. Fan, D. Y. Liu, Y. F. Wu, S. Duan, Z. X. Xie, Z. Y. Jiang, Z. Q. Tian, *J. Am. Chem. Soc.* 2008, **130**, 6949.
- 7 Y. Ding, F. R. Fan, Z. Q. Tian, Z. L. Wang, *J. Am. Chem. Soc.* 2010, **132**, 12480.
- 8 J. Yang, J. Y. Lee, H. P. Too, *J. Phys. Chem. B* 2005, **109**, 19208.
- 9 Z. Q. Tian, B. Ren, J. F. Li, Z. L. Yang, *Chem. Commun.* 2007, 3514.
- 10 P. P. Fang, J. F. Li, Z. L. Yang, L. M. Li, B. Ren, Z. Q. Tian, *J. Raman Spectrosc.* 2008, **39**, 1679.
- 11 M. F. Mrozek, Y. Xie, M. J. Weaver, *Anal. Chem.* 2001, **73**, 5953.
- 12 S. Z. Zou, M. J. Weaver, *Anal. Chem.* 1998, **70**, 2387.
- 13 R. Gomez, J. M. Perez, J. Solla-Gullon, V. Montiel, A. Aldaz, *J. Phys. Chem. B* 2004, **108**, 9943.
- 14 G. Samjeske, K. Komatsu, M. Osawa, *J. Phys. Chem. C* 2009, **113**, 10222.
- 15 V. Climent, A. Rodes, J. M. Orts, J. M. Feliu, J. M. Perez, A. Aldaz, *Langmuir* 1997, **13**, 2380.
- 16 I. Villegas, M. J. Weaver, *J. Phys. Chem. B* 1997, **101**, 5842.
- 17 M. J. Llorca, J. M. Feliu, A. Aldaz, J. Clavilier, *J. Electroanal. Chem.* 1994, **376**, 151.
- 18 F. J. Vidal-Iglesias, J. Solla-Gullon, E. Herrero, A. Aldaz, J. M. Feliu, *J. Appl. Electrochem.* 2006, **36**, 1207.
- 19 G. Q. Lu, A. Crown, A. Wieckowski, *J. Phys. Chem. B* 1999, **103**, 9700.
- 20 Y. X. Chen, M. Heinen, Z. Jusys, R. B. Behm, *Angew. Chem. Int. Ed.* 2006, **45**, 981.
- 21 G. Samjeske, A. Miki, S. Ye, M. Osawa, *J. Phys. Chem. B* 2006, **110**, 16559.
- 22 C. Yan-Tyng, Y. Yamaguchi, W. H. Miller, H. F. Schaefer, III, *J. Am. Chem. Soc.* 1987, **109**, 7245.
- 23 H. X. Zhang, C. Wang, J. Y. Wang, J. J. Zhai, W. B. Cai, *J. Phys. Chem. C* 2010, **114**, 6446.